BIOCHEMISTRY
including biophysical chemistry & molecular biology

Article

pubs.acs.org/biochemistry

Biomolecular Mode of Action of Metformin in Relation to Its Copper Binding Properties

Peter Repiščák,[†] Stefan Erhardt,[†] Graham Rena,[‡] and Martin J. Paterson*,[†]

[†]Institute of Chemical Sciences, School of Engineering and Physical Sciences, Heriot-Watt University, Edinburgh, United Kingdom EH14 4AS

[‡]Cardiovascular and Diabetes Medicine, Ninewells Hospital and Medical School, University of Dundee, Dundee, United Kingdom DD1 9SY

Supporting Information

ABSTRACT: Metformin (Metf), the most commonly used type 2 diabetes drug, is known to affect the cellular housekeeping of copper. Recently, we discovered that the structurally closely related propanediimidamide (PDI) shows a cellular behavior different from that of Metf. Here we investigate the binding of these compounds to copper, to compare their binding strength. Furthermore, we take a closer look at the electronic properties of these compounds and their copper complexes such as molecular orbital interactions and electrostatic potential surfaces. Our results clearly show that the copper binding energies cannot alone be the cause of the biochemical differentiation between Metf and PDI. We conclude that other factors such as pK_a values and hydrophilicity of the compounds play a crucial role in their cellular activity. Metf in contrast to PDI can occur as an anion in aqueous medium at moderate pH, forming much stronger complexes particularly with Cu^{II} ions, suggesting that biguanides but not PDI may induce easy oxidation of Cu^{I} ions extracted from proteins. The higher hydrophobicity and the lack of planarity of PDI may further differentiate it from biguanides in terms of their molecular recognition characteristics. These different properties could hold the key to metformin's mitochondrial activity because they suggest that the drug could act at least in part as a pro-oxidant of accessible protein-bound Cu^{I} ions.

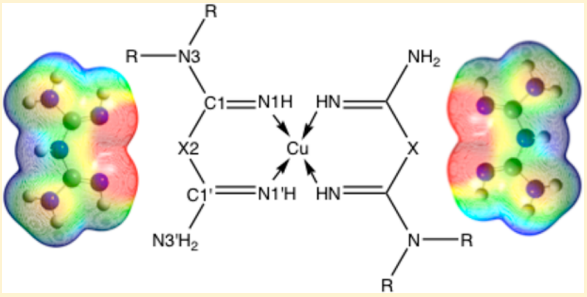

It has been estimated that more than 300 million people suffer from the diabetes worldwide.[1] By 2030 the World Health Organization estimates that diabetes will be the seventh highest cause of death.[2] Type 2 diabetes (T2D), which covers ~90% of all diabetes patients, is characterized by hyperglycaemia due to insulin resistance in peripheral tissues. One of the most effective and frequently administered antihyperglycemic T2D drugs is metformin [*N*,*N*-dimethylbiguanide, Metf (for its chemical structure, see Figure 1)], which is the first-line treatment because of better long-term outcomes compared with those of other therapies such as insulin secretagogues.[3] It belongs to the biguanide family that also includes other compounds with antihyperglycemic properties. Metf and other biguanide derivatives have been developed after it was discovered that the blood glucose-lowering ingredient in Goat's Rue is guanidine and other guanidine derivatives such as galegine. Synthalin, a diguanide, was developed as a synthetic drug and was more potent and showed lower toxicity. However, the liver damage caused by both guanidine and diguanides stimulated a search for safer alternatives, which led to the development of biguanides as T2D drugs.[3]

The exact molecular mechanism of Metf and other T2D drugs remains unclear. One suggested mechanism of action is suppression of mitochondrial respiration by inhibition of complex I;[4,5] however, the precise mechanism of this inhibition has not yet been established.

Dysfunctional copper metabolism is implicated in the development of several diseases.[6−9] Mutations in the ATP7A gene result in copper deficiency in most organs, which is the cause of Menkes's disease,[10,11] and copper overload resulting from ATP7B mutation is the cause of Wilson's disease.[12] Dysregulation of copper is also suspected in other diseases, particularly those involving protein misfolding,[13−15] and in diabetes.[16−20]

In our previous study, we demonstrated for the first time that the metal binding properties of Metf, particularly toward copper, may be one factor in cell responses to this drug.[21] Metf and biguanide (BG) show antihyperglycemic properties, and no measurable mitochondrial Cu^{II} could be detected by a Cu^{II} specific fluorescence probe. In contrast, propanediimidamide (PDI) showed no antihyperglycemic effect, and measurable Cu^{II} was detected. BG and Metf regulate AMP-activated protein kinase (AMPK), whereas PDI does not have such an effect. Regulation of S6 phosphorylation is observed for all three compounds. Interestingly, Metf does not lower the urinal

Received: October 23, 2013
Revised: January 1, 2014
Published: January 16, 2014

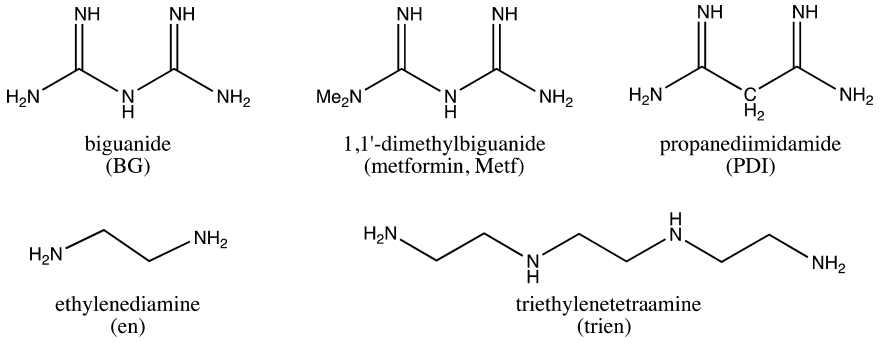

Figure 1. Compounds used as ligands.

copper concentration, which in T2D patients is increased, whereas triethylenetetraamine (trien) decreases the urinal copper concentration but has no antihyperglycemic effect.

However, it remained unclear whether Metf binds to Cu^{I} or Cu^{II}. In water, Cu^{II} is the more stable oxidation state. In living organisms, a complex machinery of cupric reductase, a Cu^{I} specific membrane transport protein, and chaperone proteins within the cells effectively does not allow free copper ions at the cellular level.[22−29] The chaperone proteins play a vital role in the copper transport system and are abundant not only in the cell but also in the mitochondria. Cu^{I} is bound to the chaperones by two cysteinates. In the unbound state, these cysteines are protonated; therefore, a perfectly designed proton array consisting of other amino acids is constructed to deprotonate the receiving chaperones or enzymes while simultaneously protonating the transporter protein to lower its copper binding affinity. Moreover, copper metalloenzymes, in which the unique copper redox chemistry is needed, are able to bind both Cu^{I} and Cu^{II}. Therefore, there are various possibilities of interaction of the drug with $Cu^{I/II}$ proteins, and Metf could potentially interact with protein-bound $Cu^{I/II}$ ions.

There are major differences in the coordination chemistry of Cu^{I} and Cu^{II}. In the lower oxidation state, Cu^{I} prefers binding to soft ligands such as thiols, thiolates (cysteine), or thioethers (methionine) or sp^2-containing nitrogen (histidine). On the other hand, Cu^{II} favors binding to slightly harder ligands such as amines and imines. According to Pearson's hard and soft acids and bases (HSAB) concept, Cu^{I} is classified as a soft acid whereas Cu^{II} is classified as an intermediate acid.[30−33] Also, Cu^{I} has two to four ligand atoms in the first coordination sphere compared to three to six for Cu^{II}. Generally, a tetrahedral coordination sphere is observed for Cu^{I}, whereas a square planar ligand orientation is commonly found for Cu^{II}.[34,35] In an enzymatic environment, a mixed coordination sphere of sulfur- and nitrogen-containing ligands assist to stabilize Cu^{I} and at the same time facilitate the reversible redox chemistry of $Cu^{I/II}$.

Similar to the imidazole residue in histidine, a sp^2-hybridized N1 (for atom labels, see Figure 2) is the ligand atom for BG, Metf, and PDI. This means that π-backbonding can occur and stabilize the lower Cu^{I} oxidation state by transferring electron density into the π-orbitals of the ligands (see Figure 3). This type of molecular orbital (MO) interaction may also be important for Cu^{II} as its 3d orbitals are almost filled up. The methylene CH_2 moiety in PDI compared to secondary amine N2 in BG and Metf causes a disruption of the π-system, whereas the lone pair of N2 can contribute electron density to the adjacent carbon p_z orbital in BG and Metf, which results in a planar molecular structure for the latter compounds and a

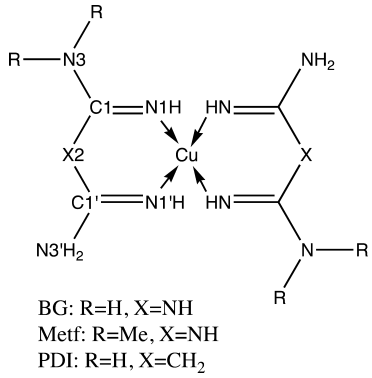

Figure 2. Numbering of atoms in X-ray and computed structures.

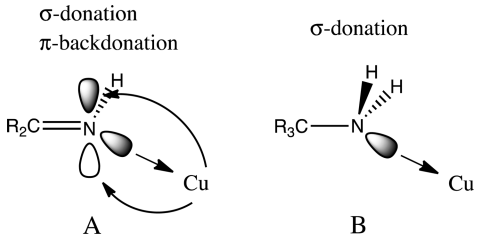

Figure 3. Schematic representation of possible orbital interactions of Cu complexes with BG, Metf, and PDI (A) and with en and trien (B).

nonplanar geometry for PDI in the complex. This is similar to the stabilization effect detected in peptide bonds.

Additionally, the N2H group contains a protic hydrogen, whereas the methylene hydrogens cannot undergo proton exchange in aqueous media. Deprotonated metal complexes of PDI are known; however, those are synthesized in nonprotic solvents under conditions that prevent any water contamination.[36−38] Because of the protic hydrogen, the most stable neutral form of BG and Metf in water is a tautomer in which the proton of the N2H group is formally transferred to N1 or N3.[39] This leads to a fully conjugated π-system in the ligands. However, only N2 can then act as a donor atom as has been observed with a similar ligand in a known Ag^{I} complex.[40]

Biguanides formally belong to the 1,3,5-triazapentadienyl[41,42] (also known as imidoylamidine) ligand family, and PDI is a member of the 1,5-diazapentadienyl[35,38,43] (also known as β-diketiminate) ligand class, each of which is well established as a metal ion ligand in inorganic coordination chemistry. However, their structure and chemistry are mainly established in nonaqueous solvents; hence, their properties cannot be transferred directly to aqueous environments, particularly biosystems with a very sensitive pH range.

dx.doi.org/10.1021/bi401444n | Biochemistry 2014, 53, 787−795

Table 1. Comparison of Critical Bonds[a] (distances in angstroms) of $[Cu^{II}(BG)_2]X_{1,2}$ {X = CO_3^{2-}, Cl^-, or $[Cu^{II}(C_5H_7O_2)(Cl)]^-$} and $Cu^{II}(BG\text{-}H)_2$ Crystal Structures and Computed $[Cu^{II}(BG/BG\text{-}H)_2]^{2+/0}$ Complexes

BG	CSD code	X	Cu−N	N1−C1	C1−N2	C1−N3
X-ray	BGCUCB[60]	CO_3^{2-}	1.951	1.296	1.374	1.351
	COBMAH[61]	$[Cu^{II}(C_5H_7O_2)(Cl)]^-$	1.936	1.287	1.372	1.337
	ZZZDZQ01[62]	Cl^-	1.941	1.289	1.373	1.342
	Ø[b]{$[Cu(BG)_2]^{2+}$}		1.944	1.292	1.373	1.344
	STD		0.011	0.009	0.009	0.012
	MUE		0.023	0.016	0.017	0.018
B3LYP	$[Cu(BG)_2]^{2+}$		1.980	1.299	1.383	1.344
X-ray	SAPFUL[63]	–	1.941	1.320	1.355	1.360
B3LYP	$Cu(BG\text{-}H)_2$		1.971	1.318	1.337	1.383

[a]Experimental bond lengths are averaged for each crystal structure (BGCUCB C_1 symmetry, COBMAH C_i symmetry, and ZZZDZQ01 C_1 symmetry). [b]Average of all $[Cu^{II}(BG)_2]X_{1,2}$ structures.

The protonation equilibria of BG have been studied along with complex formation with Cu^{II} over a pH range of 2−12.[44,45] First, BG predominately exists in an equilibrium between its monoprotonated and neutral forms at physiological pH, and no deprotonated BG-H was reported for the given pH range. Second, the formation of $[Cu^{II}(OH)(BG)]^+$ was observed to be the major Cu−BG complex; however, binary Cu^{II}−BG complexes such as $[Cu(BG)_2]^{2+}$, $[Cu(BG)(BG\text{-}H)]^+$, and $[Cu(BG\text{-}H)_2]^0$ were also observed at slightly higher pH values. A pK_a value of 6.88 was reported for $[Cu(OH)(BG)]^+$, hence indicating the possibility of deprotonated BG while being coordinated to Cu^{II}. Neither Metf nor PDI has been studied in this detail. However, these results are at least qualitatively transferred to Metf.

In a recent study, the antimicrobial properties of binary metformin metal complexes were studied.[46,47] Among other physicochemical properties, the cyclic voltammogram of $[Cu^{II}(Metf)_2]^{2+}$ was measured against a Ag/AgCl electrode and showed a reduction peak at 320 mV and an oxidation peak at 490 mV, giving an $E_{1/2}$ of 405 mV, which is in the range of the reduction potentials of copper-containing enzymes.[48]

Here we aim to build upon our previous work on the cellular response to T2D drugs and in particular on the observed variations of free copper levels after drug treatment. We gain deeper insight into the copper binding properties of BG and Metf with a focus on possible differences with respect to PDI, which may be important for their different biological antihyperglycemic properties. We compute binding energies and compare the optimized structures to known crystal structures, in the process benchmarking the computational methodology for such systems. Furthermore, we will investigate the electronic properties such as molecular orbitals and electrostatic potentials of these molecules.

MATERIALS AND METHODS

Computational Details. Geometries of all the computed structures were obtained by optimization with B3LYP.[49−53] Basis set Def2-TZVPD[54] was used for all atoms. For Cu(I) complexes, singlet spin multiplicity was used, while for Cu(II), doublet spin multiplicity was used. For the open-shell species, spin contamination was found to be negligible. Each structure was verified to be a minimum by the absence of imaginary frequencies in the vibrational analysis. The calculations were performed using Gaussian 09 A.02 and C.01.[55] We also tested other DFT functionals, including BP86,[51,56] M06,[57] and M06L,[58] which showed no significant difference from B3LYP. Natural bond orbital (NBO) charges were calculated with the integrated NBO 3.1[59] program within Gaussian 09.

RESULTS

Comparison of X-ray Structures and Computed Complexes. Several crystal structures of bisbiguanide−copper complexes are known. Three describe the $[Cu(BG)_2]^{2+}$ complex and contain different counterions.[60−62] Although these complexes are planar, they are not symmetric in terms of their bond lengths. An average over all three structures is presented in Table 1 and will be discussed here in comparison to the DFT-optimized structure. One structure for the $Cu(BG\text{-}H)_2$ neutral complex that contains the deprotonated biguanide (BG-H) has been published.[63] The deprotonation was confirmed by visual inspection of H bond contacts to the deprotonated N2$^-$.

The observed Cu−N1 bond length (1.944 Å) is in the normal range of Cu^{II}−N ligand bonds. The computed Cu−N bond distance (1.980 Å) is slightly longer; however, this is expected and is a known effect when computing complexes in the gas phase and comparing them to crystal structures. Also, the Cu−N bond length in the different crystal structures can vary from 1.921 to 1.958 Å for complexes with the neutral BG ligand. The most symmetrical, coplanar X-ray structure COBMAH[61] is C_i symmetric with Cu−N distances of 1.933 and 1.939 Å. This feature is reproduced by the DFT calculation with slightly different Cu−N bonds of 1.978 and 1.982 Å. Interestingly, the computed minimum energy structure is slightly twisted and has C_2 symmetry with regard to the heavy atoms, which is abolished by the nonplanar H atoms of the amine groups. The coplanar, D_{2h} symmetrical geometry is in fact computed to be a rotational transition state in the gas phase with a negligible barrier $\Delta E^{\ddagger}$ of 1.04 and a $\Delta G^{\ddagger}$ of 3.65 kcal/mol.

The observed N1−C1 bond length (X-ray$_{av}$, 1.292 Å; DFT, 1.299 Å) is slightly longer than a pure C−N double bond, whereas the C1−N2 (X-ray$_{av}$, 1.373 Å; DFT, 1.383 Å) and C1−N3 (X-ray$_{av}$, 1.343 Å; DFT, 1.344 Å) bonds are much shorter than a C−N single bond, which indicates conjugation of the N2 lone pairs into the N1−C1 double bound. The computed N−C bonds are in much better agreement with the crystal structure compared to the metal−ligand bond because these bonds are less affected by crystal packing. In particular, the changes upon deprotonation of the secondary amine N2H group in the N1−C1 and C1−N2 bonds that indicate a delocalization of the negative charge within the ligand bonds that form the metallacycle is very well reproduced in the

Table 2. Comparison of Critical Bonds[a] (distances in angstroms) of $[Cu^{II}(Metf)_2]X_{1,2}$ (X = ClO_4^-, CO_3^{2-}, or Cl^-) and $Cu^{II}(Metf\text{-}H)_2$ Crystal Structures and Computed Complexes

Metf	CSD code	X	Cu−N1	Cu−N1′	N1−C1	N1′−C1′	C1−N2	C1′−N2	C1−N3	C1′−N3′
X-ray	AJUHUJ[47]	ClO_4^-	1.944	1.944	1.303	1.268	1.374	1.384	1.354	1.344
	HIBPOX[68]	CO_3^{2-}	1.931	1.920	1.305	1.282	1.364	1.393	1.342	1.322
	HIHDUX[69]	Cl^-	1.948	1.931	1.307	1.279	1.377	1.379	1.342	1.344
	Ø{$[Cu(Metf)_2]^{2+}$}		1.941	1.932	1.305	1.276	1.372	1.385	1.346	1.337
	STD		0.009	0.012	0.002	0.007	0.007	0.007	0.007	0.013
	MUE		0.010	0.012	0.002	0.008	0.008	0.008	0.008	0.015
B3LYP	$[Cu(Metf)_2]^{2+}$		1.973	1.980	1.307	1.298	1.389	1.379	1.346	1.348
X-ray	EFIXUM[64]	–	1.943	1.921	1.312	1.306	1.372	1.350	1.365	1.386
	ETOFOI[65]-A[a]	–	1.938	1.928	1.324	1.320	1.358	1.350	1.368	1.371
	ETOFOI[65]-B[a]	–	1.950	1.923	1.315	1.310	1.371	1.342	1.357	1.391
	Ø$[Cu(Metf\text{-}H)_2]$		1.944	1.924	1.317	1.312	1.367	1.347	1.363	1.383
	STD		0.006	0.004	0.006	0.007	0.008	0.005	0.006	0.010
	MUE		0.006	0.004	0.007	0.008	0.009	0.005	0.006	0.012
B3LYP	$Cu(Metf\text{-}H)_2$		1.970	1.967	1.323	1.320	1.343	1.332	1.383	1.388

[a]The unit cell of ETOFOI contains two $Cu(Metf\text{-}H)_2$ molecules.

Table 3. Comparison of Critical Structural Parameters (bond distances in angstroms and angles in degrees) of $[Cu^{II}(PDI)_2][ClO_4]_2$ Crystal Structures and Computed $[Cu^{II}(PDI/PDI\text{-}H)_2]^{2+/0}$ Complexes

PDI	CSD code	X	Cu−N	N1−C1	C1−C2	C1−N3	∠N1−N2−C3−C2[†]
X-ray	MALDOU[66]	ClO_4^-	1.956	1.288	1.501	1.332	21.6
B3LYP	$[Cu(PDI)_2]^{2+}$		1.999	1.297	1.514	1.336	22.1
	$[Cu(PDI\text{-}H)_2]^0$		1.976	1.321	1.403	1.394	1.4

computed structure. The observed differences between the different X-ray structures are possibly explained by the different counterions. Remarkably, an almost negligible shortening of −0.002 Å for the Cu−N bond length is observed for the $Cu(BG\text{-}H)_2$ neutral complex[63] compared to the average of the cationic complexes, whereas the DFT calculations reveal a stronger reduction of −0.009 Å, indicating a much larger increase in the Cu−N bond strength than the experimental results are suggesting.

With respect to the Metf−Cu complexes, in total five crystal structures are known (see Table 2); three include the neutral Metf[47,64,65] and two the deprotonated metformin (Metf-H)[64,65] with Cu^{II}. Some differences compared to the BG-Cu complexes in the bond distances can be observed and are due to the methyl groups that abolish the symmetry of the BG complex. The N1−C1 bond becomes slightly longer ($X\text{-}ray_{av}$, 1.305 Å; DFT, 1.307 Å) and the N1′−C1′ bond slightly shorter ($X\text{-}ray_{av}$, 1.276 Å; DFT, 1.298 Å) than the N1−C1 bond ($X\text{-}ray_{av}$, 1.291 Å; DFT, 1.299 Å) in the BG complex. This alteration is also observed in the computed complex, although the decrease in the N1′−C1′ bond is only marginal. The asymmetrical nature of the ligand is also noticeable in different Cu−N bond distances (Cu−N1, 1.942 Å; Cu−N1′, 1.929 Å); surprisingly, the DFT computed Cu−N bond distances show an opposite trend with values of 1.973 and 1.980 Å, which might be due to crystal packing effects compared to the gas-phase computed, single-molecule structure. However, the other bond distances are in excellent agreement.

The two crystal structures of $Cu^{II}(Metf\text{-}H)_2{\cdot}H_2O$ (ETOFOI)[65] and $Cu(Metf\text{-}H)_2{\cdot}8H_2O$ (EFIXUM)[64] were synthesized under basic conditions. The ETOFOI structure complex contains two $Cu^{II}(Metf\text{-}H)_2$ molecules in the unit cell, with ETOFOI-A resembling the $Cu^{II}(BG\text{-}H)_2$ more closely than ETOFOI-B and EFIXUM. The best agreement with the DFT-optimized $Cu(Metf\text{-}H)_2$ structure is also with ETOFOI-A. The lengthened N1−C1 and N1′−C1′ double bond is particularly well reproduced by the B3LYP-optimized structure.

Surprisingly, in EFIXUM and ETOFOI-B, hardly any increase in the N1−C1 bond length or decrease in the C1−N2 bond length is observed, which most likely is due to strong H-bonding of crystal water in the proximity of N2. Two crystal waters are close two N2⁻ atoms in EFIXUM at distances of 2.86 and 2.91 Å (N2−O distance), whereas one water is found in ETOFOI-B to be 2.84 Å from N2⁻.

Overall, the crystal structures of the neutral complex $Cu^{II}(Metf\text{-}H)_2$ indicate the possibility of the formation of stable Cu^{II} complex with deprotonated metformin at basic conditions.

Only one crystal structure for the homoleptic PDI complex is known.[66] The Cu−N bond (1.956 Å) in the $[Cu^{II}(PDI)_2]^{2+}$ complex is slightly longer than in the BG complex (1.943 Å), which is also observed in the computed structure (1.999 Å for PDI and 1.980 Å for BG). In contrast to those of the BG complexes, the C1−C2 bond (1.501 Å) in the PDI complex is much longer than the C1−N2 bond (1.373 Å) in $[Cu^{II}(BG)_2]^{2+}$ and closer to a pure single C−C bond than a double bond.

Intrigued by this long C1−C2 bond, we calculated the rotational barrier of the free, neutral ligand of 2.42 kcal/mol for PDI and 18.20 kcal/mol for BG. The much higher rotational barrier for BG gives an indication of the strength of the conjugation of the N2 lone pair into the adjacent N1−C1 double bond.

Binding Energies of $Cu^{I/II}$ Complexes. The binding energies that are listed in Table 2 were computed in two different ways. The interaction energy ΔE_{int} corresponds to the binding energy of the Cu center or CuOH fragment with the ligand in its geometry found in the optimized complex structure. On the other hand, the binding free energy ΔG is determined using the lowest-energy tautomer and conformer of

dx.doi.org/10.1021/bi401444n | Biochemistry 2014, 53, 787−795

Table 4. Binding Energies (kilocalories per mole) of Cu Complexes (B3LYP/Def2-TZVPD)

		BG	Metf	PDI	en	trien
$[Cu^{I}(L)]^{+}$	ΔE_{int}	−119.77	−125.07	−120.74	−95.15	
	ΔG (=$-D_e$)	−84.71	−87.45	−94.18	−78.60	
$[Cu^{II}(L)]^{2+}$	ΔE_{int}	−331.77	−347.81	−332.66	−270.92	
	ΔG (=$-D_e$)	−286.23	−299.91	−296.49	−250.70	
$[Cu^{I}(L)_2]^{+}$	ΔE_{int}	−183.80	−187.80	−186.28	−154.32	−151.04
	ΔG (=$-D_e$)	−105.97	−106.64	−124.85	−112.52	−117.58
$[Cu^{II}(L)_2]^{2+}$	ΔE_{int}	−489.52	−505.09	−488.51	−410.06	−409.90
	ΔG (=$-D_e$)	−391.59	−402.19	−405.96	−355.32	−364.10
$[Cu^{I}(OH)(L)]$	ΔE_{int}	−50.88	−47.80	−51.05	−42.10	
	ΔG (=$-D_e$)	−16.26	−12.02	−34.12	−24.60	
$[Cu^{II}(OH)(L)]^{+}$	ΔE_{int}	−138.25	−144.61	−138.73	−112.33	
	ΔG (=$-D_e$)	−97.37	−101.23	−105.93	−88.99	
$[Cu^{I}(L\text{-}H)]$	ΔE_{int}	−229.86	−231.38	−234.86		
	ΔG (=$-D_e$)	−200.71	−201.60	−203.80		
$[Cu^{II}(L\text{-}H)]^{+}$	ΔE_{int}	−555.26	−561.38	−566.70		
	ΔG (=$-D_e$)	−511.20	−518.40	−530.24		
$[Cu^{I}(L\text{-}H)_2]^{-}$	ΔE_{int}	−353.80	−351.71	−359.31		
	ΔG (=$-D_e$)	−220.55	−220.70	−218.21		
$[Cu^{II}(L\text{-}H)_2]$	ΔE_{int}	−836.32	−837.06	−846.10		
	ΔG (=$-D_e$)	−678.65	−680.45	−680.12		

the ligands. The negative ΔG is equal to the dissociation energy D_e. The difference between the energy of the ligand in its complex geometry and its lowest tautomer and conformer is called preparation energy ΔE_{prep} (Table 3).

We have computed binding energies for Cu^{I} and Cu^{II} complexes of the mono-L complexes, the homoleptic, bis-L complexes, and the mixed $[Cu^{I/II}(OH)(L)]^{0/+}$ complexes (Table 4). The latter is particularly important in aqueous media as this is the major Cu^{II}−BG species at physiological pH in most biological compartments. We also calculated the complexes with deprotonated ligands as this might become important at higher physiological pH values, occurring, for example, inside mitochondria.

First, the $[Cu^{I/II}(L)]^{+/2+}$ complexes are discussed. Among all ligands, Metf shows the strongest interaction energy with Cu^{I}; however, because of the lower ΔE_{prep}, PDI forms the strongest $[Cu^{I}(L)]^{+}$ complex. Interestingly, for BG and PDI, ΔE_{int} is almost equal. En binds around 25−30 kcal/mol weaker to Cu^{I} compared to the other ligands, but D_e is only 6−16 kcal weaker, which is also due to a small preparation energy. The weaker binding of en is due to the lack of π-backbonding, and also larger steric strain as en forms a five-membered metallacycle compared to the six-membered metallacycle of the BG−, Metf−, and PDI−Cu complexes.

The Cu^{II} complexes for BG, Metf, and PDI are more than 200 kcal/mol more stable than the Cu^{I} complex, which is due to stronger Coulomb and orbital interactions, whereas the en complex is not as strongly stabilized compared to the other ligands. This could be due to two factors; the σ-bonding with the N lone pair is smaller in the sp^3 hybrid N compared to the slightly larger sp^2 hybid lone pair with more s-character. The other factor, although this plays a minor role, is the possibility of the occupied ligand π-orbitals donating electron density to the Cu d^9 center. Overall, Metf binds strongest; however, the D_e of PDI is only 3.4 kcal/mol lower.

Second, we will consider the homoleptic $[Cu^{I/II}(L)_2]^{+/2+}$ complexes. For BG, Metf, and PDI complexes, we observe trends similar to those seen for the monocomplexes, with an even stronger stabilization for PDI compared to BG and Metf due to a much larger ΔE_{prep} for the latter two. We also include trien in this group of complexes. Obviously because trien is tetradentate, its chelating properties are superior to those of BG, Metf and PDI at equal molarity; however, we are more interested in its binding properties in comparison to copper−ligand complexes with a saturated copper ligand sphere. Trien has almost the same ΔE_{int} as en, but a larger D_e due to entropic effects of 5 kcal/mol with Cu^{I} and ∼10 kcal/mol with Cu^{II}, which agrees with the experimentally observed stronger stabilization of trien with Cu^{II}.

Next we will investigate the binding of BG, Metf, PDI, and en in a mixed complex with Cu(OH), where OH is a stronger ligand than the neutral, bidentate ligands. The Cu^{I} cation forms a strong bond with the hydroxide anion, which results in weak binding of a second, non-anionic ligand. Here we observe a surprising order for the Cu^{I} complexes. PDI forms the strongest mixed complexes; en follows as the second strongest, and then BG and Metf form the weakest complex. The differences between the ligands are again mainly due to the larger ΔE_{prep} for BG and Metf compared to the low ΔE_{prep} for PDI and en.

The mixed $Cu^{II}(OH)(L)$ complexes are slightly stronger than the $Cu^{I}(L)$ complexes, with very similar trends and similar stabilities for BG, Metf, and PDI.

In addition to the complexes with neutral ligands, we have also calculated the binding energies for the deprotonated BG-H, Metf-H, and PDI-H species. It is important to point out here that at higher pH values BG and Metf can be deprotonated in aqueous medium, whereas PDI, even when in a metal complex that lowers its pK_a, will only be deprotonated above pH 14 in nonaqueous medium as the methylene group in PDI cannot be deprotonated by bases in aqueous media.

These anionic ligands bind much stronger than the neutral counterparts as they have much larger ionic bonding contributions than the neutral ligands. Also, the Cu^{II} complexes receive an even stronger stabilization than the Cu^{I} complexes. This could indicate an easier oxidation compared to the neutral ligands when a Cu^{I} ion is extracted from a protein by Metf-H. In addition, these deprotonated forms of the biguanides alone might be strong enough as ligands to extract Cu^{I} from proteins

dx.doi.org/10.1021/bi401444n | Biochemistry 2014, 53, 787−795

with thiolate ligands. This modeling indicates that any copper-dependent effects of the drug may be restricted to or most prominent in the mitochondria and other compartments in the body where physiological pH is above the typical range, allowing deprotonation of the drug. Such pH-dependent activation or priming could potentially explain why metformin is almost invariably found in the biological literature to act on the mitochondria, with very few effects reported in other cellular compartments.

Electronic Properties. To gain a deeper understanding of the biguanide type ligands compared to PDI, we take a look at the molecular orbitals (MOs) of these ligands in their geometry in a complex (see Figure 4). For the sake of simplicity, we will concentrate on the π-orbitals and the MOs with the N1 lone pairs.

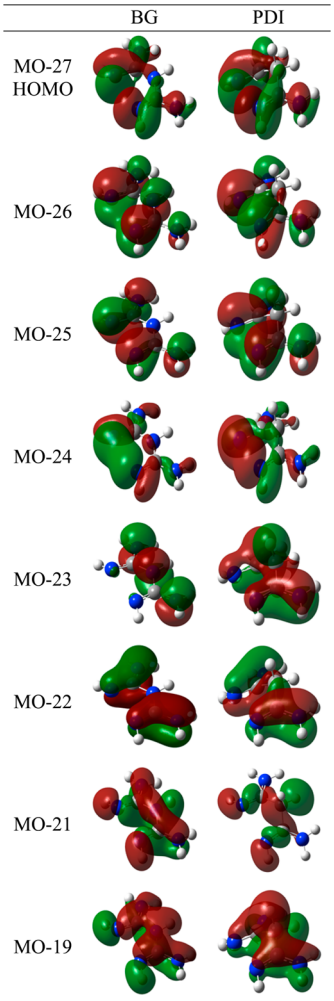

Figure 4. Molecular orbitals for BG and PDI.

The lowest-lying MO with π-character in BG and PDI is MO-19. PDI, which is not planar, still shows a π-like plane with one σ-C2−H bond above and the other σ-C2−H bond mixing with the N1−C1 double bond plus a contribution from the N3 lone pairs. MO-19 in BG is a mix of π- and σ-character. The lone pairs of N2 and N3 are mixing with the p_z AO of the sp^2-hybridized C1, plus σ-character from the N1−H bond. For BG, MO-21 looks very similar to MO-19 with σ- and π-character, except that it is the negative combination of the AOs and therefore has a higher energy. MO-21 in PDI shows only σ-character, which explains the much lower rotational barrier for PDI compared to that for BG. MO-22 is basically the same for both molecules. MO-23 in BG is a pure combination of N2 and N3 lone pairs, whereas in PDI, as there is no lone pair on C2, this MO is a mix of π-MO with contributions from the N1−C1 double bonds and the N3 lone pairs plus out-of-plane C2−H σ-bond character. MO-24 is the positive combination of the N1 lone pairs that is responsible for bonding to the empty 4s AO of Cu. The next two MOs, 25 and 26, are identical for BG and PDI and are pure π-MOs. The HOMO, MO-27, is the negative combination of the N1 lone pairs and donates electron density into the empty 4p AO of Cu. These MOs show that the electron density on N1 is very similar in BG and PDI, which explains the strong similarities in the observed binding energies for these ligands with Cu.

To emphasize this point, we calculated the NBO charges for the $[Cu(L)]^{2+}$ complexes (Table 5). The charges on Cu are +1.87, +1.84, and +1.80 for BG, PDI, and en, respectively. This is consistent with a decreasing negative charge on the ligand N1 atoms of these ligands (−0.87, −0.84, and −0.80, respectively). Figure 2 illustrates the possible orbital interactions for the sp^2 type N in BG, Metf, and PDI compared to the sp^3 type N in en and trien. The former are capable of stronger bonds due to σ-donation while at the same time receiving electron density from the metal center via π-backdonation; these two types of bonding have a synergistic effect and reinforce each other. On the other hand, the pure σ-donor ligands en and trien cannot accept electron density in π-MOs, which results in weaker binding. The small difference between BG and PDI can be due to either slightly larger σ-donation, smaller π-backdonation in PDI, or a combination of both.

Table 5. NBO Charges for $[Cu^{II}(L)]^{2+}$ (L = BG, PDI, or en)

	BG	PDI	en
Cu^{II}	+1.38	+1.34	+1.30
N1	−0.87	−0.84	−0.80

ESP Maps. The electrostatic potential (ESP) maps for BG and PDI in their neutral forms are presented in Figure 5. Interestingly, PDI-A shows a slightly more negative potential around the N1 atoms that will form coordination bonds toward Cu. This means that PDI is a slightly stronger Lewis base than BG-A and is consistent with our findings that the PDI has a larger ΔE_{int}. It has to be pointed out here that the presented structure of PDI-A is not a minimum energy structure and therefore not stable in nature; however, this is the conformation that will bind to a metal center in a bidentate binding mode. BG-A, on the other hand, is a minimum energy structure, which also is in one sense surprising as the two N1 lone pairs should strongly repel each other; however, it seems that the p-stabilization as shown by the MOs exceeds the steric repulsion. Also, the methylene moiety causes a greater part of PDI-A to be hydrophobic compared to BG-A, which could be important in terms of molecular recognition when binding to a Cu center of a protein. Therefore, PDI not only causes greater steric hindrance because of its lack of planarity but also introduces repulsive or at least weaker interactions with H-bond acceptors.

PDI-B represents the lowest-energy conformer of the neutral PDI. An internal H-bond in PDI-B results in a very weak hydrophilicity, with strong, large areas that can be described as lipophilic. In contrast, BG-B, which is not the lowest tautomer of BG, shows much more pronounced negative and positive

dx.doi.org/10.1021/bi401444n | Biochemistry 2014, 53, 787−795

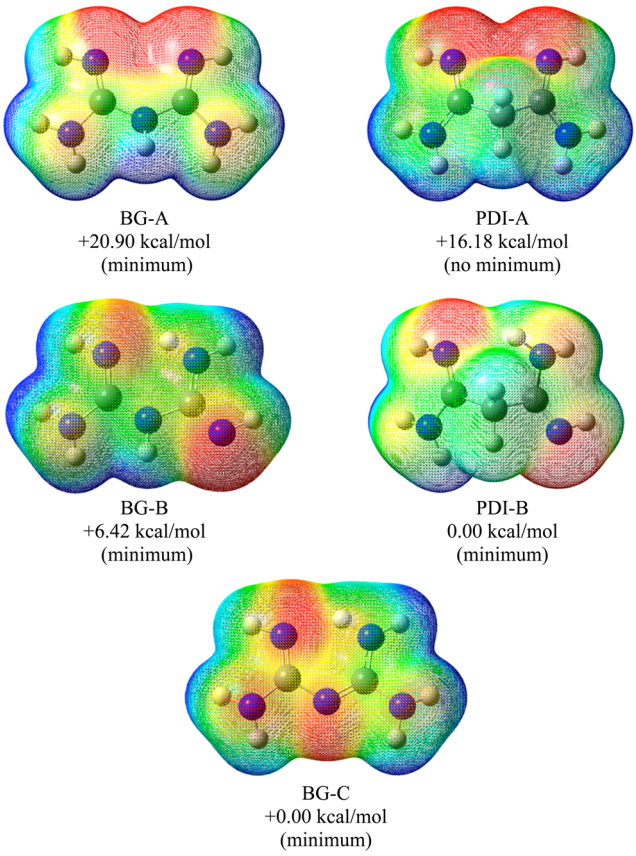

Figure 5. Electrostatic potential maps for BG and PDI. Red indicates negative ESP values, green neutral ESP values, and blue positive ESP values.

moieties, which results in H-bond donor and acceptor properties that are stronger than those of PDI-B. This is suggestive evidence that PDI may be able to penetrate cell membranes, whereas BG and Metf need to be taken up via transmembrane transporters.

The lowest-energy conformer and tautomer of BG-C does not show Lewis acid or basic sites as strong as those of BG-B; however, there are also fewer hydrophobic areas above the plane of the molecules, which means that solvation and stabilization due to H-bonding can be stronger not only on the edges of the molecules but also along the molecular plane.

DISCUSSION

In this study, we find that the biologically observed differences between neutral biguanide compounds (BG and Metf) and PDI cannot be explained by different Cu binding energies. These ligands are too electronically similar, and the substitution of the secondary amine with methylene has no negative effect on the complex formation via the N1 atoms for PDI. However, the secondary amine of biguanides can be deprotonated in aqueous medium as the pK_a value is reduced when BG or Metf is coordinated to $Cu^{I/II}$. These anions form much stronger complexes than their neutral form. It is known that the mitochondrial matrix pH is higher than the normal cellular or serum pH. Inside the mitochondria, it is possible that the equilibrium is shifted toward the $Cu^{I/II}$(Metf-H) complex. Extraction of Cu^{I} ions from proteins is possible, and subsequent oxidation to Cu^{II} would remove the redox active Cu^{I} ions from the mitochondria. This suggests that metformin could act in cells at least in part as a copper-binding prodrug, becoming activated by elevated mitochondrial pH values. This is consistent with the strong emphasis on the mitochondrial effects of this drug in the biological literature. In addition, this probably explains the differences between mitochondrial responses to metformin and PDI, as the latter agent becomes deprotonated only at much higher pH values. There is a possibility that high binding affinities of Metf-H for copper could significantly affect the mitochondrial copper pool, which would probably have an impact on metal homeostasis of other metals and lead to mis-metalation of important metalloproteins.[67] The redox properties of such copper complexes may interfere with the sensitive redox chemistries occurring inside the cell, such as the mitochondrial electron transport chain.

Furthermore, ESP maps show that molecular recognition processes, which are copper-independent, could play a vital role in explaining the different drug properties of biguanides and PDI. Further work will establish if the much stronger hydrophilicity of BG facilitates its mitochondrial activity. On the other hand, we showed the higher lipophilicity of PDI, which might allow it to penetrate cell membranes without relying on membrane transport proteins.

In summary, these calculations clearly demonstrate that metformin is a pH-sensitive copper-binding agent with a pK_a within the physiological pH range and a strongly hydrophilic character. Together, these properties of metformin distinguish it from the other copper-binding agents we have studied, and they are also likely to account for many of the biological/therapeutic responses to the drug.

ASSOCIATED CONTENT

Supporting Information

Optimized geometries and corresponding energies for Tables 1 and 2. This material is available free of charge via the Internet at http://pubs.acs.org.

AUTHOR INFORMATION

Corresponding Author

*E-mail: m.j.paterson@hw.ac.uk. Phone: +44(0)131 451 8035.

Funding

M.J.P. and P.R. thank the European Research Council for funding under the European Union's Seventh Framework Programme (FP7/2007-2013)/ERC Grant 258990. M.J.P. and S.E. thank the Leverhulme Trust for funding through Research Grant RPG-165. G.R. acknowledges support from MRC and Diabetes UK.

Notes

The authors declare no competing financial interest.

ABBREVIATIONS

AMP, 5′-adenosine monophosphate; AMPK, AMP-activated protein kinase; AO, atomic orbital; B3LYP, Becke−3−Lee−Yang−Parr density functional; BG, biguanide; BG-H, deprotonated biguanide; CSD, Cambridge Structural Database; DFT, density functional theory; en, ethylenediamine; ESP, electrostatic potential; MO, molecular orbital; Metf, metformin (*N*,*N*-dimethylbiguanide); Metf-H, deprotonated metformin; NBO, natural bond orbital; PDI, propanediimidamide; T2D, type 2 diabetes; trien, triethylenetetraamine.

REFERENCES

(1) Danaei, G., Finucane, M. M., Lu, Y., Singh, G. M., Cowan, M. J., Paciorek, C. J., Lin, J. K., Farzadfar, F., Khang, Y.-H., Stevens, G. A., Rao, M., Ali, M. K., Riley, L. M., Robinson, C. A., and Ezzati, M. (2011) National, regional, and global trends in fasting plasma glucose and diabetes prevalence since 1980: Systematic analysis of health examination surveys and epidemiological studies with 370 country-years and 2.7 million participants. *Lancet 378*, 31−40.

(2) Mathers, C. D., and Loncar, D. (2006) Projections of global mortality and burden of disease from 2002 to 2030. *PLoS Med. 3*, No. e442.

(3) Rena, G., Pearson, E. R., and Sakamoto, K. (2013) Molecular mechanism of action of metformin: Old or new insights? *Diabetologia 56*, 1898−1906.

(4) El-Mir, M. Y., Nogueira, V., Fontaine, E., Averet, N., Rigoulet, M., and Leverve, X. (2000) Dimethylbiguanide inhibits cell respiration via an indirect effect targeted on the respiratory chain complex I. *J. Biol. Chem. 275*, 223−228.

(5) Owen, M. R., Doran, E., and Halestrap, A. P. (2000) Evidence that metformin exerts its anti-diabetic effects through inhibition of complex 1 of the mitochondrial respiratory chain. *Biochem. J. 348*, 607−614.

(6) Camakaris, J., Voskoboinik, I., and Mercer, J. F. (1999) Molecular mechanisms of copper homeostasis. *Biochem. Biophys. Res. Commun. 261*, 225−232.

(7) Linder, M. C., and HazeghAzam, M. (1996) Copper biochemistry and molecular biology. *Am. J. Clin. Nutr. 63*, S797−S811.

(8) Olivares, M., and Uauy, R. (1996) Copper as an essential nutrient. *Am. J. Clin. Nutr. 63*, S791−S796.

(9) Xu, W., Barrientos, T., and Andrews, N. C. (2013) Iron and Copper in Mitochondrial Diseases. *Cell Metab.*, 319−328.

(10) Kaler, S. G., Buist, N. R. M., Holmes, C. S., Goldstein, D. S., Miller, R. C., and Gahl, W. A. (1995) Early copper therapy in classic Menkes disease patients with a novel splicing mutation. *Ann. Neurol. 38*, 921−928.

(11) Madsen, E., and Gitlin, J. D. (2007) Copper deficiency. *Curr. Opin. Gastroenterol. 23*, 187−192.

(12) Scheinberg, I. H., and Sternlieb, I. (1996) Wilson disease and idiopathic copper toxicosis. *Am. J. Clin. Nutr. 63*, S842−S845.

(13) Christen, Y. (2000) Oxidative stress and Alzheimer disease. *Am. J. Clin. Nutr. 71*, 621S−629S.

(14) Cobb, N. J., and Surewicz, W. K. (2009) Prion diseases and their biochemical mechanisms. *Biochemistry 48*, 2574−2585.

(15) Eskici, G., and Axelsen, P. H. (2012) Copper and oxidative stress in the pathogenesis of Alzheimer's disease. *Biochemistry 51*, 6289−6311.

(16) Masad, A., Hayes, L., Tabner, B. J., Turnbull, S., Cooper, L. J., Fullwood, N. J., German, M. J., Kametani, F., El-Agnaf, O. M. A., and Allsop, D. (2007) Copper-mediated formation of hydrogen peroxide from the amylin peptide: A novel mechanism for degeneration of islet cells in type-2 diabetes mellitus? *FEBS Lett. 581*, 3489−3493.

(17) Gybina, A. A., and Prohaska, J. R. (2008) Fructose-2,6-bisphosphate is lower in copper deficient rat cerebellum despite higher content of phosphorylated AMP-activated protein. *Exp. Biol. Med. 233*, 1262−1270.

(18) Gybina, A. A., and Prohaska, J. R. (2008) Copper deficiency results in AMP-activated protein kinase activation and acetylCoA carboxylase phosphorylation in rat cerebellum. *Brain Res. 1204*, 69−76.

(19) Tanaka, A., Kaneto, H., Miyatsuka, T., Yamamoto, K., Yoshiuchi, K., Yamasaki, Y., Shimomura, I., Matsuoka, T. A., and Matsuhisa, M. (2009) Role of copper ion in the pathogenesis of type 2 diabetes. *Endocr. J. 56*, 699−706.

(20) Dosa, M. D., Hangan, L. T., Crauciuc, E., Gales, C., and Nechifor, M. (2011) Influence of therapy with metformin on the concentration of certain divalent cations in patients with non-insulin-dependent diabetes mellitus. *Biol. Trace Elem. Res. 142*, 36−46.

(21) Logie, L., Harthill, J., Patel, K., Bacon, S., Hamilton, D. L., Macrae, K., McDougall, G., Wang, H.-H., Xue, L., Jiang, H., Sakamoto, K., Prescott, A. R., and Rena, G. (2012) Cellular responses to the metal-binding properties of metformin. *Diabetes 61*, 1423−1433.

(22) Boal, A. K., and Rosenzweig, A. C. (2009) Structural biology of copper trafficking. *Chem. Rev. 109*, 4760−4779.

(23) Bertini, I., and Rosato, A. (2003) Bioinorganic chemistry in the postgenomic era. *Proc. Natl. Acad. Sci. U.S.A. 100*, 3601−3604.

(24) Puig, S., and Thiele, D. J. (2002) Molecular mechanisms of copper uptake and distribution. *Curr. Opin. Chem. Biol. 6*, 171−180.

(25) Rubino, J. T., and Franz, K. J. (2012) Coordination chemistry of copper proteins: How nature handles a toxic cargo for essential function. *J. Inorg. Biochem. 107*, 129−143.

(26) Nose, Y., Rees, E. M., and Thiele, D. J. (2006) Structure of the Ctr1 copper trans'PORE'ter reveals novel architecture. *Trends Biochem. Sci. 31*, 604−607.

(27) Abajian, C., Yatsunyk, L. A., Ramirez, B. E., and Rosenzweig, A. C. (2004) Yeast Cox17 solution structure and copper(I) binding. *J. Biol. Chem. 279*, 53584−53592.

(28) Horn, D., and Barrientos, A. (2008) Mitochondrial copper metabolism and delivery to cytochrome c oxidase. *IUBMB Life 60*, 421−429.

(29) Wang, Y. F., Hodgkinson, V., Zhu, S., Weisman, G. A., and Petris, M. J. (2011) Advances in the understanding of mammalian copper transporters. *Adv. Nutr. 2*, 129−137.

(30) Pearson, R. G. (1963) Hard and soft acids and bases. *J. Am. Chem. Soc. 85*, 3533−3539.

(31) Pearson, R. G. (1968) Hard and soft acids and bases, HSAB, part I: Fundamental principles. *J. Chem. Educ. 45*, 581−587.

(32) Pearson, R. G. (1968) Hard and soft acids and bases, HSAB, part II: Underlying theories. *J. Chem. Educ. 45*, 643−648.

(33) Parr, R. G., and Pearson, R. G. (1983) Absolute hardness: Companion parameter to absolute electronegativity. *J. Am. Chem. Soc. 105*, 7512−7516.

(34) Huheey, J. E., Keiter, E. A., and Keiter, R. L. (1993) *Inorganic chemistry: Principles of structure and reactivity*, HaperCollins College Publisher, New York.

(35) Solomon, E. I., Szilagyi, R. K., DeBeer George, S., and Basumallick, L. (2004) Electronic structures of metal sites in proteins and models: Contributions to function in blue copper proteins. *Chem. Rev. 104*, 419−458.

(36) Feldman, J., McLain, S. J., Parthasarathy, A., Marshall, W. J., Calabrese, J. C., and Arthur, S. D. (1997) Electrophilic metal precursors and a β-diimine ligand for nickel(II)- and palladium(II)-catalyzed ethylene polymerizations. *Organometallics 16*, 1514−1516.

(37) Holland, P. L., and Tolman, W. B. (1999) Three-coordinate Cu(II) complexes: Structural models of trigonal-planar type 1 copper protein active sites. *J. Am. Chem. Soc. 121*, 7270−7271.

(38) Randall, D. W., George, S. D., Holland, P. L., Hedman, B., Hodgson, K. O., Tolman, W. B., and Solomon, E. I. (2000) Spectroscopic and electronic structural studies of blue copper model complexes. 2. Comparison of three- and four-coordinate Cu(II)-thiolate complexes and fungal laccase. *J. Am. Chem. Soc. 122*, 11632−11648.

(39) Bharatam, P. V., Patel, D. S., and Iqbal, P. (2005) Pharmacophoric features of biguanide derivatives: An electronic and structural analysis. *J. Med. Chem. 48*, 7615−7622.

(40) Dias, H. V. R., and Singh, S. (2004) Silver(I) complexes of a sterically demanding fluorinated triazapentadienyl ligand $[N\{(C_3F_7)C(Dipp)N\}_2]^-$ (Dipp 2,6-diisopropylphenyl). *Inorg. Chem. 43*, 7396−7402.

(41) Flores, J. A., and Dias, H. V. R. (2008) Gold(I) ethylene and copper(I) ethylene complexes supported by a polyhalogenated triazapentadienyl ligand. *Inorg. Chem. 47*, 4448−4450.

(42) Kopylovich, M. N., and Pombeiro, A. J. L. (2011) Coordination chemistry of 1,3,5-triazapentadienes. *Coord. Chem. Rev. 255*, 339−355.

(43) Randall, D. W., George, S. D., Holland, P. L., Hedman, B., Hodgson, K. O., Tolman, W. B., and Solomon, E. I. (2000) Spectroscopic and electronic structural studies of blue copper model complexes. 2. Comparison of three- and four-coordinate Cu(II)-

thiolate complexes and fungal laccase. *J. Am. Chem. Soc. 122*, 11632−11648.
(44) Barman, T. R., and Mukherjee, G. N. (2006) Mixed-ligand complex formation equilibria of Cu-II with biguanide in presence of glycine as the auxiliary ligand. *J. Chem. Sci. (Bangalore, India) 118*, 411−418.
(45) Barman, T. R., and Mukherjee, G. N. (2009) Coordination equilibria of mixed ligand complexes of Cu-II with glycylglycine and biguanide. *Indian J. Chem., Sect. A: Inorg., Bio-inorg., Phys., Theor. Anal. Chem. 48*, 38−44.
(46) Olar, R., Badea, M., Marinescu, D., Chifiriuc, C. M., Bleotu, C., Grecu, M. N., Iorgulescu, E. E., Bucur, M., Lazar, V., and Finaru, A. (2010) Prospects for new antimicrobials based on N,N-dimethylbiguanide complexes as effective agents on both planktonic and adhered microbial strains. *Eur. J. Med. Chem. 45*, 2868−2875.
(47) Olar, R., Badea, M., Marinescu, D., Chifiriuc, M.-C., Bleotu, C., Grecu, M. N., Iorgulescu, E.-E., and Lazar, V. (2010) N,N-Dimethylbiguanide complexes displaying low cytotoxicity as potential large spectrum antimicrobial agents. *Eur. J. Med. Chem. 45*, 3027−3034.
(48) Solomon, E. I., Szilagyi, R. K., George, S. D., and Basumallick, L. (2004) Electronic structures of metal sites in proteins and models: Contributions to function in blue copper proteins. *Chem. Rev. 104*, 419−458.
(49) Becke, A. D. (1993) Density-functional thermochemistry. III. The role of exact exchange. *J. Chem. Phys. 98*, 5648−5652.
(50) Stephens, P. J., Devlin, F. J., Chabalowski, C. F., and Frisch, M. J. (1994) Ab initio calculation of vibrational absorption and circular dichroism spectra using density functional force fields. *J. Phys. Chem. 98*, 11623−11627.
(51) Becke, A. D. (1988) Density-functional exchange-energy approximation with correct asymptotic behavior. *Phys. Rev. A 38*, 3098−3100.
(52) Vosko, S. H., Wilk, L., and Nusair, M. (1980) Accurate spin-dependent electron liquid correlation energies for local spin density calculations: A critical analysis. *Can. J. Phys. 58*, 1200−1211.
(53) Lee, C., Yang, W., and Parr, R. G. (1988) Development of the Colle-Salvetti correlation-energy formula into a functional of the electron density. *Phys. Rev. B 37*, 785−789.
(54) Rappoport, D., and Furche, F. (2010) Property-optimized Gaussian basis sets for molecular response calculations. *J. Chem. Phys. 133*, 134105−134111.
(55) Frisch, M. J., Trucks, G. W., Schlegel, H. B., Scuseria, G. E., Robb, M. A., Cheeseman, J. R., Scalmani, G., Barone, V., Mennucci, B., Petersson, G. A., Nakatsuji, H., Caricato, M., Li, X., Hratchian, H. P., Izmaylov, A. F., Bloino, J., Zheng, G., Sonnenberg, J. L., Hada, M., Ehara, M., Toyota, K., Fukuda, R., Hasegawa, J., Ishida, M., Nakajima, T., Honda, Y., Kitao, O., Nakai, H., Vreven, T., Montgomery, J. A., Jr., Peralta, J. E., Ogliaro, F., Bearpark, M., Heyd, J. J., Brothers, E., Kudin, K. N., Staroverov, V. N., Kobayashi, R., Normand, J., Raghavachari, K., Rendell, A., Burant, J. C., Iyengar, S. S., Tomasi, J., Cossi, M., Rega, N., Millam, J. M., Klene, M., Knox, J. E., Cross, J. B., Bakken, V., Adamo, C., Jaramillo, J., Gomperts, R., Stratmann, R. E., Yazyev, O., Austin, A. J., Cammi, R., Pomelli, C., Ochterski, J. W., Martin, R. L., Morokuma, K., Zakrzewski, V. G., Voth, G. A., Salvador, P., Dannenberg, J. J., Dapprich, S., Daniels, A. D., Farkas, Ö., Foresman, J. B., Ortiz, J. V., Cioslowski, J., and Fox, D. J. (2009) *Gaussian 09*, Gaussian, Inc., Wallingford, CT.
(56) Perdew, J. P. (1986) Density-functional approximation for the correlation energy of the inhomogeneous electron gas. *Phys. Rev. B 33*, 8822−8824.
(57) Zhao, Y., and Truhlar, D. (2008) The M06 suite of density functionals for main group thermochemistry, thermochemical kinetics, noncovalent interactions, excited states, and transition elements: Two new functionals and systematic testing of four M06-class functionals and 12 other functionals. *Theor. Chem. Acc. 120*, 215−241.
(58) Zhao, Y., and Truhlar, D. G. (2006) A new local density functional for main-group thermochemistry, transition metal bonding, thermochemical kinetics, and noncovalent interactions. *J. Chem. Phys. 125*, 194101−194118.
(59) Glendening, E. D., Reed, A. E., Carpenter, J. E., and Weinhold, F. *NBO*, version 3.1.
(60) Coghi, L., Lanfranchi, M., Pelizzi, G., and Tarasconi, P. (1978) Structural researches on the chelating behaviour of the biguanide ligand. The crystal structures of $Co(C_2H_6N_5)_3\cdot 2H_2O$ and $Cu(C_2H_7N_5)_2CO_3\cdot 4H_2O$. *Transition Met. Chem. (Dordrecht, Neth.) 3*, 69−76.
(61) Hota, S. K., Saha, C. R., and Pritzkow, H. (1984) Syntheses and properties of some 5-coordinate and 6-coordinate copper(II) complexes with acetylacetonate and the structural characterization of a biguanide-acetylacetonate double salt. *J. Coord. Chem. 13*, 131−142.
(62) Kennard, C. H. L., Smith, G., and O'Reilly, E. J. (1983) The crystal and molecular structure of bis(biguanide)copper(II) chloride dihydrate. *Inorg. Chim. Acta 77*, L113−L115.
(63) Su, Y. L., Lu, L. P., Li, X. M., and Zhu, M. L. (2005) Bis(biguanido-κ^2-N,N′)copper(II) dihydrate. *Acta Crystallogr. E61*, m910−m912.
(64) Zhu, M., Lu, L., Yang, P., and Jin, X. (2002) Bis(1,1-dimethylbiguanido)copper(II) octahydrate. *Acta Crystallogr. E58*, m217−m219.
(65) Lu, L. P., Yang, P., Qin, S. D., and Zhu, M. L. (2004) Bis[1,1-dimethylbiguanide(1-)-κ^2N^2,N^5]copper(II) monohydrate. *Acta Crystallogr. C60*, m219−m220.
(66) Schwarzenbach, D., and Schmelczer, R. (1978) Comparison of an OD and an ordered structure of nickel and copper malondiamidine complexes. *Acta Crystallogr. B34*, 1827−1833.
(67) Pierrel, F., Cobine, P. A., and Winge, D. R. (2007) Metal ion availability in mitochondria. *BioMetals 20*, 675−682.
(68) Viossat, B., Tomas, A., and Dung, N.-H. (1995) L'hydrogenocarbonate de Bis(N,N-dimethylbiguanide) Cuivre(II), $[Cu(C_4H_{11}N_5)_2]_2HCO_3$. *Acta Crystallogr. C51*, 213−215.
(69) Lemoine, P., Chiadmi, M., Bissery, V., Tomas, A., and Viossat, E. (1996) Les Composés de la Metformine avec les Ions Co(II), Cu(II) et Ni(II). *Acta Crystallogr. C52*, 1430−1436.